GEOCHEMISTRY

The redox "filter" beneath magmatic orogens and the formation of continental crust

Ming Tang,* Monica Erdman, Graham Eldridge, Cin-Ty A. Lee*

The two most important magmatic differentiation series on Earth are the Fe-enriching tholeiitic series, which dominates the oceanic crust and island arcs, and the Fe-depleting calc-alkaline series, which dominates the continental crust and continental arcs. It is well known that calc-alkaline magmas are more oxidized when they erupt and are preferentially found in regions of thick crust, but why these quantities should be related remains unexplained. We use the redox-sensitive behavior of europium (Eu) in deep-seated, plagioclase-free arc cumulates to directly constrain the redox evolution of arc magmas at depth. Primitive arc cumulates have negative Eu anomalies, which, in the absence of plagioclase, can only be explained by Eu being partly reduced. We show that primitive arc magmas begin with low oxygen fugacities, similar to that of mid-ocean ridge basalts, but increase in oxygen fugacity by over two orders of magnitude during magmatic differentiation. This intracrustal oxidation is attended by Fe depletion coupled with fractionation of Fe-rich garnet. We conclude that garnet fractionation, owing to its preference for ferrous over ferric iron, results in simultaneous oxidation and Fe depletion of the magma. Favored at high pressure and water content, garnet fractionation explains the correlation between crustal thickness, oxygen fugacity, and the calc-alkaline character of arc magmas.

INTRODUCTION

There is a long-standing debate on what controls the oxidized nature of arc magmas, particularly those formed in continental arcs (*1*, *2*). This debate has profound implications for Earth's evolution because oxidized arc magmas, manifested in the form of iron-depleted magmas, are the primary building blocks of the continental crust (*3*). The debate is centered on whether the oxidized signatures of arc magmas are inherited from the mantle source or developed during magmatic differentiation, crustal interaction, or degassing. Iron and sulfur oxidation states in melt inclusions have been used to suggest that fluids released from the subducted slab pervasively oxidize the sub-arc mantle, producing oxidized arc magmas from the onset (*1*, *4*, *5*), but redox-sensitive trace element ratios and Fe isotope signatures of basalts, which have been used to see through eruptive and differentiation processes, suggest that primitive arc magmas are not as oxidized as widely thought (*6*–*8*). None of the above studies, however, represent direct constraints on the oxidation state of primitive, pre-erupted magmas.

Here, we examine the Eu systematics of deep-seated (>45 to 80 km) garnet pyroxenite continental arc cumulates to provide the most direct constraint so far on arc magmas before they rise into the crust or erupt. Europium is a rare earth element (REE), but unlike most other REEs, which are exclusively trivalent under typical terrestrial conditions, Eu occurs in both divalent and trivalent states, so the ratio of Eu^{2+}/Eu^{3+} is sensitive to variations in oxygen fugacity (fO_2). Although Eu^{2+} strongly partitions into plagioclase, in all other magmatic minerals, Eu^{2+} is more incompatible than Eu^{3+} and neighboring REEs, making the total partitioning of Eu sensitive to fO_2. Eu^{2+}/Eu^{3+} may be a more robust redox-sensitive index than element pairs, such as V/Sc (*9*) and Zn/Fe (*7*), because the geochemical behavior of both Eu^{2+} and Eu^{3+} can be well constrained throughout magmatic differentiation. Eu systematics in plagioclase-free rocks can thus be used to constrain the Eu valence state, which in turn can be used to estimate oxygen fugacity using experimentally calibrated Eu oxybarometers (*10*).

Department of Earth, Environmental and Planetary Sciences, Rice University, Houston, TX 77005, USA.
*Corresponding author. Email: tangmyes@gmail.com (M.T.); ctlee@rice.edu (C.-T.A.L.)

RESULTS

We sampled garnet-bearing pyroxenite xenoliths from Miocene trachyandesitic volcanic centers on the margin of the Colorado Plateau in Arizona (*11*, *12*). They have major element compositions complementary to typical continental arc plutonic rocks and are thus interpreted to represent arc cumulates (*11*). These deep cumulates do not contain any evidence of plagioclase. Titanite U/Pb systematics suggest crystallization in the Late Cretaceous or Early Paleogene (*11*). Their mineralogies and trace and major element signatures are identical to arc cumulates associated with the Cretaceous Sierra Nevada batholith toward the west (*11*, *13*, *14*). The Arizona garnet pyroxenites are thus interpreted to represent cumulates from hydrous arc magmas associated with Mesozoic to Early Cenozoic arc magmatism in western North America (*11*). They have Mg#s [atomic Mg/(Mg+Fe), where Fe represents total Fe] ranging from 0.5 to 0.82, the latter representing early formed cumulates from primitive arc magmas and the former representing cumulates from more evolved magmas (see the Supplementary Materials and Methods).

The deep petrogenetic origins of the garnet pyroxenites and the lack of any visible evidence for plagioclase make these pyroxenites ideal for applying Eu systematics as an oxybarometer of arc magmas before eruption. To avoid potential contamination of the whole-rock xenolith by recent injection of Miocene host lavas onto grain boundaries, we performed in situ laser ablation ICP-MS (inductively coupled plasma mass spectrometry) analyses of garnets and clinopyroxenes in thin sections (see the Supplementary Materials and Methods). Longer dwell times on Sm, Gd, and Eu were applied to increase the precision and accuracy of the analyses.

Oxygen fugacity of primitive arc magmas constrained by mineral Eu anomalies

Europium valence can be quantified from the relative difference (the Eu anomaly) in geochemical behavior between Eu^{2+} and neighboring REEs. Eu anomalies are expressed as Eu/Eu*, where Eu* represents the hypothetical concentration of Eu if it behaved solely like a trivalent REE and is calculated by polynomial interpolation of REE systematics in the order of their ionic radii (see the Supplementary Materials and

Methods). We find that both clinopyroxene and garnet show increasing Eu/Eu* with decreasing Mg# (Fig. 1), a measure of the extent of differentiation. This negative correlation is consistent with Eu^{2+} being more incompatible than Eu^{3+} and is also consistent with plagioclase being absent during the entire crystallization history of these cumulates because plagioclase fractionation would decrease Eu/Eu* with differentiation. Because of the lack of plagioclase, the fact that the most primitive cumulates have Eu/Eu* <1 is interesting. Global compilations of arc magmas show that primitive arc magmas have Eu/Eu* of unity (see the Supplementary Materials and Methods); only after MgO contents decrease to levels below 6 weight % (wt %) does Eu/Eu* deviate from unity due to the onset of plagioclase fractionation (*15*). In conclusion, the negative Eu anomalies of the primitive arc cumulates can only be explained if Eu is of mixed valence.

We now use the Eu/Eu* of the most primitive arc cumulates (CC-ME1, whole-rock Mg# = 0.77; SB1-ME9, Mg# = 0.82) to calculate the Eu valence state, which in turn allows us to place an upper bound on the fO_2 of primitive arc magmas (Fig. 2A). The Eu/Eu* of a mineral is controlled by the composition of the melt (including the melt's Eu/Eu* and Eu^{2+}/Eu^{3+}) and the ratio of the mineral/melt partitioning of Eu^{2+} ($D^{\text{min-melt}}_{\text{Eu(II)}}$) to Eu^{3+} ($D^{\text{min-melt}}_{\text{Eu(III)}}$). From mass balance, Eu valence in the melt ($Eu^{3+}/\Sigma Eu$) can be calculated using the following equation (derivation in the Supplemental Materials)

$$\frac{Eu^{3+}}{\sum Eu} = \frac{(Eu/Eu^{*}_{min})/(Eu/Eu^{*}_{melt}) - D^{\text{min-melt}}_{\text{Eu(II)}}/D^{\text{min-melt}}_{\text{Eu(III)}}}{1 - D^{\text{min-melt}}_{\text{Eu(II)}}/D^{\text{min-melt}}_{\text{Eu(III)}}} \quad (1)$$

Eq. 1 assumes that the mineral is in equilibrium with the melt (subsolidus reequilibration in garnet-pyroxenites has minimal effect on mineral Eu/Eu* because Eu^{2+} is highly incompatible in garnet). $D^{\text{min-melt}}_{\text{Eu(III)}}$ is estimated from the behavior of trivalent REEs, whereas $D^{\text{min-melt}}_{\text{Eu(II)}}$ can be estimated from the behavior of geochemically similar Sr^{2+}. In clinopyroxene, $D^{\text{cpx-melt}}_{\text{Eu(II)}}/D^{\text{cpx-melt}}_{\text{Eu(III)}}$ can be equated to $D_{Sr}/\sqrt{D_{Sm} * D_{Gd}}$, which ranges between 0.03 and 1.53 with a median value of 0.22 (n = 89, excluding kimberlites and carbonatites) based on published partition coefficients (*16*). Additional constraints come from clinopyroxenes in ureilite meteorites, wherein most of the Eu is divalent due to the highly reducing conditions of ureilites (*17*). Ureilite clinopyroxenes have Eu/Eu* ranging from 0.18 to 0.63 with a median value of 0.29 (n = 49), and assuming that parental magmas begin with Eu/Eu^{*}_{melt} = 1, the measured Eu/Eu* values in ureilites provide an upper bound of ~0.2 on $D^{\text{cpx-melt}}_{\text{Eu(II)}}/D^{\text{cpx-melt}}_{\text{Eu(III)}}$. In garnet, Sr is highly incompatible, which is consistent with the pyroxenite garnets having Sr barely above detection limits (0.1 to 1 parts per million); $D^{\text{gt-melt}}_{\text{Eu(II)}}/D^{\text{gt-melt}}_{\text{Eu(III)}}$ is thus effectively zero in garnet, simplifying Eq. 1. In the extreme case, in which $D^{\text{min-melt}}_{\text{Eu(II)}}$ = 0 for all minerals, Eq. 1 simplifies such that the ratio of the Eu anomaly in the pyroxenite versus that in the melt provides a maximum bound on the $Eu^{3+}/\Sigma Eu$ ratio.

We use both clinopyroxene and garnet in the most primitive cumulates to estimate the Eu valence state of the primitive magma. As noted above, the primitive magma is assumed to have Eu/Eu^{*}_{melt} = 1. We can use experimentally calibrated Eu^{2+}/Eu^{3+}–fO_2 relationships in silicate melts (*10*) to obtain fO_2. Details of the calculation are provided in the Supplementary Materials. Garnets and clinopyroxenes in CC-ME1 give

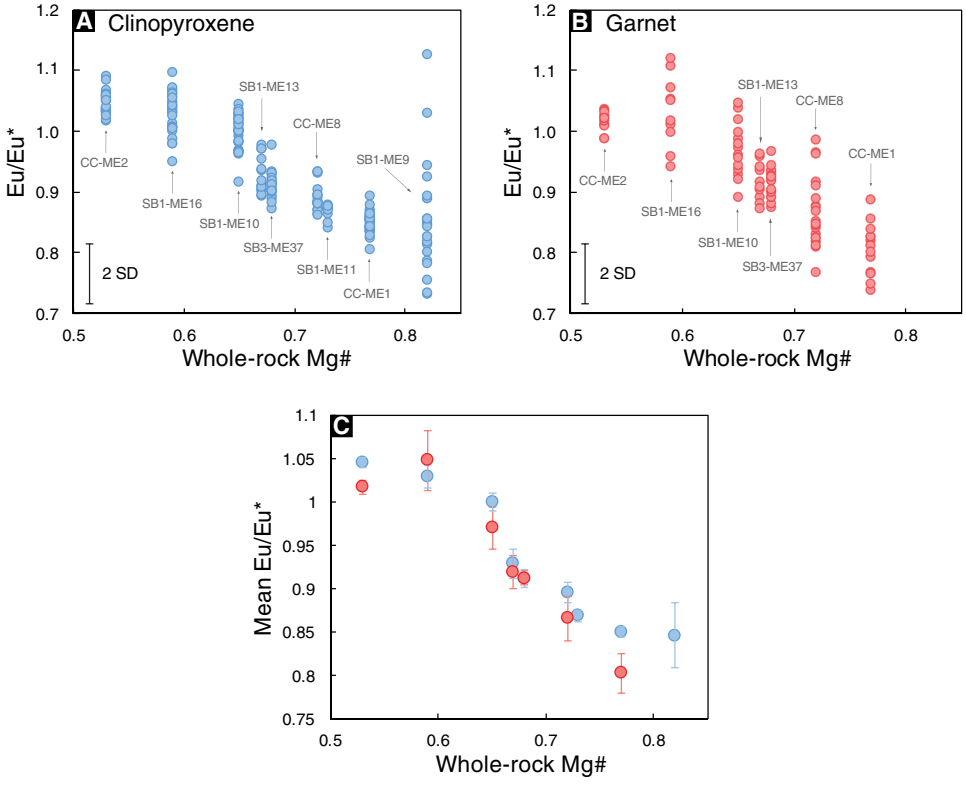

Fig. 1. Eu/Eu* in clinopyroxene and garnet in deep arc cumulates as a function of whole-rock Mg#. (**A** and **B**) Individual spot data measured by laser ablation ICP-MS. The error bars denoted in (A) and (B) are the long-term (~8 months) reproducibilities (2 SD) of measuring Eu/Eu* in basaltic glass standards BIR-1G and BCR-2G. (**C**) The mean Eu/Eu* in clinopyroxene and garnet for each rock sample. Error bars are 2 standard error of mean (2 SEM).

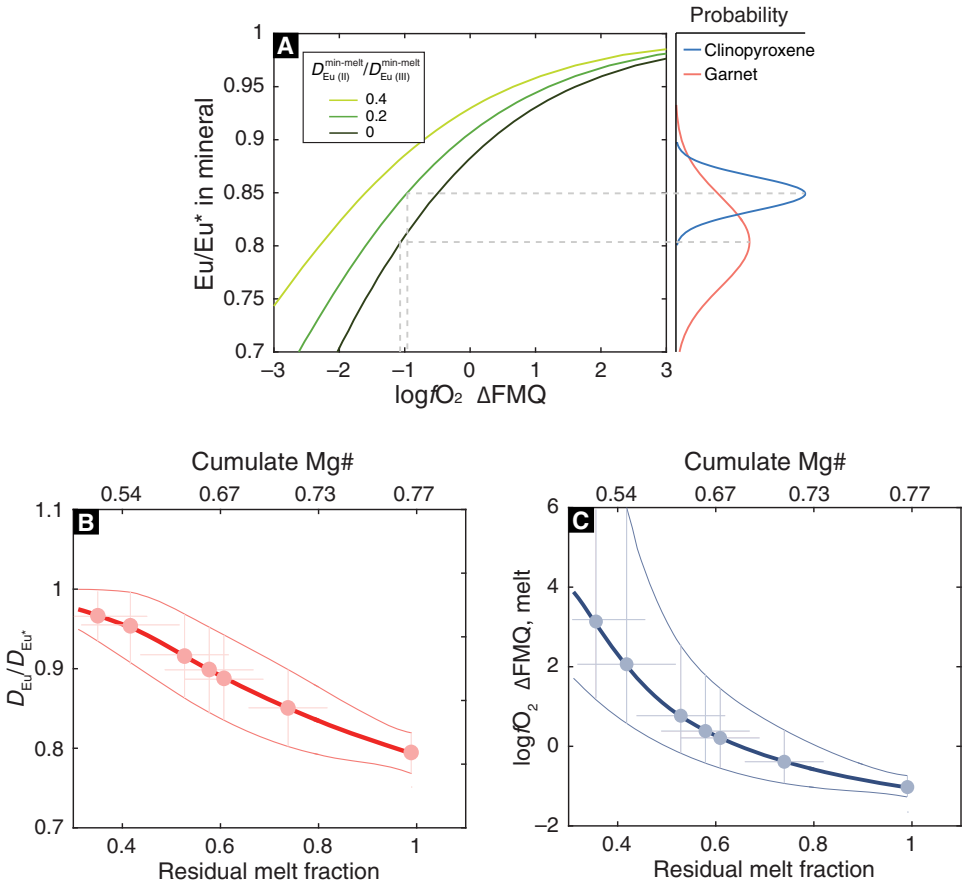

Fig. 2. Magma redox conditions calculated from garnet and clinopyroxene Eu anomalies. (**A**) Estimating fO_2 of primitive magma. Garnet and clinopyroxene Eu/Eu*-fO_2 plotted on the contours of $D_{Eu(II)}^{min\text{-}melt}/D_{Eu(III)}^{min\text{-}melt}$. The probability distribution is for sample CC-ME1, the second most primitive garnet-bearing pyroxenite in this work. (**B**) Evolution of the bulk Eu partition coefficient relative to D_{Eu^*} (bulk partition coefficient of Eu^{3+}) during crystal fractionation, calculated using the observed Eu/Eu* of garnets and an incremental crystal fractionation model (see the Supplementary Materials and Methods). Dots with error bars (95% confidence interval) represent D_{Eu}/D_{Eu^*} values estimated from Eu/Eu* of garnets in cumulates. Residual melt fraction estimated by converting whole-rock cumulate Mg# to the Mg# of a melt in equilibrium with the cumulate and inferring melt fraction from empirical relationships between melt Mg# and indices of melt fraction, such as K_2O (see the Supplementary Materials and Methods). The uncertainties are from the measured garnet Eu/Eu* and cumulate-melt Mg# coupling and are propagated into the calculated D_{Eu}/D_{Eu^*} and fO_2 by a Monte Carlo resampling method (see the Supplementary Materials and Methods). Thick red line demarcates median values, and thin red line displays 95% confidence interval envelope. The total Eu partition coefficients in (B) were converted to fO_2 in (C). Clinopyroxenes show the same Eu/Eu*-Mg# trend as garnet (Fig. 1), but we use garnet data to calculate the redox paths because the perfect incompatibility of Eu^{2+} in garnet simplifies Eq. 1 and reduces uncertainty.

similar magma fO_2 values of −1.0 (±1.0, 2 SD) and −1.0 (±0.5, 2 SD) $\log_{10}$ units relative to the fayalite-magnetite-quartz (FMQ) buffer (Fig. 2A), identical to within error that inferred from mid-ocean ridge basalts (FMQ−1 to FMQ) (*18*–*20*). If garnet and clinopyroxene $D_{Eu(II)}^{min\text{-}melt}/D_{Eu(III)}^{min\text{-}melt}$ ratios are higher than those used here, which seems unlikely, even lower fO_2 values would be estimated (Fig. 2A). Sample SB1-ME9 has too few garnets to investigate while clinopyroxenes show significant scatter in Eu/Eu* (Fig. 1A) due to uncertainties associated with extremely low REE concentrations (tens of parts per billion Eu). Nevertheless, the mean Eu/Eu* of SB1-ME9 clinopyroxenes is identical to those of CC-ME1 (Fig. 1C). We thus use CC-ME1 to constrain the maximum fO_2 in primitive arc magmas.

Redox evolution of arc magmas during differentiation

We now turn to the increase of Eu/Eu* with decreasing Mg#. This trend reflects the enrichment of more incompatible Eu^{2+} in the melt and/or rising fO_2 with differentiation. Progressive crystal fractionation leads to a predictable decrease in the Mg# of the melt and cumulate (see the Supplementary Materials and Methods). Using a semiempirical relationship between Mg# of the cumulate and residual melt fraction relative to a primitive mantle-derived magma to estimate the residual melt fraction corresponding to each cumulate, we can estimate the mineral/melt partition coefficient at any given Mg# by incrementally crystallizing cumulates. This inverse approach allows us to identify how the cumulate/melt bulk Eu partition coefficient, calculated as D_{Eu} relative to D_{Eu^*} (D_{Eu}/D_{Eu^*}; Fig. 2B), varies with crystallization in the cumulates. The D_{Eu}/D_{Eu^*} ratio, which reflects the Eu^{2+}/Eu^{3+} ratio in the melt, is then converted to fO_2 (Fig. 2C) using experimental constraints (*10*).

In the foregoing calculations, we assume a bulk cumulate-melt partition coefficient of 0.5 for Eu^{3+} (D_{Eu^*}), which is likely a maximum bound based on published mineral-melt partition coefficients of Eu^{3+} for clinopyroxene (*21*) and garnet (*22*). In the Supplementary Materials, we vary the value of D_{Eu^*} (0.2 to 0.8) to test the sensitivity of our model to D_{Eu^*}. If the value of D_{Eu^*} is lower than that used here, calculated

magma fO_2 rises more rapidly with differentiation, so our estimates of fO_2 during differentiation are minimum bounds. On the basis of this analysis, we find that fO_2 increased from FMQ−1 to at least FMQ+1 with crystal fractionation of these garnet pyroxenite cumulates (Fig. 2C). Our observations suggest that the fO_2 of the sub-arc mantle may not be significantly different from that beneath mid-ocean ridges and that the oxidized signature of arc magmas may be acquired during ascent and differentiation.

DISCUSSION

The initially low fO_2 inferred for primitive arc magmas raises the question of what drives the Fe depletion characterizing calc-alkaline series differentiation. Iron depletion, which distinguishes the calc-alkaline series from the tholeiitic series, is generally attributed to early magnetite fractionation in oxidized magmas. However, if primitive arc magmas are reduced, magnetite saturation will be suppressed initially (*23*) and magmatic differentiation should follow the Fe-enriching tholeiitic series unless the magma becomes oxidized during differentiation. Resolving this calc-alkaline paradox thus requires an intracrustal process that simultaneously depletes Fe and oxidizes the residual melt.

There are several ways to oxidize magmas in the crust. Assimilation of oxidized crustal materials is one possibility, but the origin and abundance of oxidized materials in deep arc crust are enigmatic if primitive arc magmas—the building blocks of arc crust—are reduced. Coupled fractional crystallization and recharge in magma chambers has also been invoked to explain Fe^{3+} enrichment in arc magma differentiation (*24*), but whether such a process can explain early Fe depletion is unclear.

Some hints come from the well-known, but incompletely understood, observation that immature island arcs are predominantly tholeiitic, whereas continental arcs mostly generate calc-alkaline magmas (*25*–*30*). These compositional relationships with crustal thickness are also reflected by the magma FeO_T-MgO correlations in global arcs (Fig. 3). If these different differentiation trends are controlled by crustal thickness, it seems worthwhile to explore whether the average pressure of differentiation, by controlling the crystallizing assemblage (*27*, *31*–*33*), may influence magma redox evolution.

Magma redox conditions are largely controlled by the Fe^{3+}/Fe^{2+} ratio because Fe is generally the most abundant source of electron transfer in most magmas. Therefore, melt redox will be dictated by the bulk solid/liquid partition coefficient ratio $D_{Fe\ (III)}/D_{Fe\ (II)}$. We use pMELTS (*34*), a thermodynamic melting model, to simulate crystal fractionation of a hydrous basaltic melt (see the Supplementary Materials and Methods) at pressures between 0.2 and 2.0 GPa, corresponding to the range of crustal thickness from tholeiitic island arcs (~20 km) to calc-alkaline continental arcs (50 to 80 km).

At low pressure, Fe is moderately incompatible in olivine and clinopyroxene and strongly incompatible in plagioclase, so crystallization leads to Fe enrichment. Although Fe^{3+} is generally incompatible in Fe-bearing silicates, the low-pressure silicate fractionating phases incorporate limited Fe (Fig. 4A). Furthermore, the combination of crystallizing low $Fe^{3+}/\Sigma Fe$ silicate phases with high $Fe^{3+}/\Sigma Fe$ iron oxide phases limits the extent to which crystal fractionation at low pressure can increase magma redox state.

On the other hand, as pressure increases, the Fe-bearing crystallizing assemblage transitions from olivine + clinopyroxene + spinel/magnetite to garnet + clinopyroxene (Fig. 4A). At high pressure, garnet is the major Fe-bearing phase and removes up to ~50% of the total initial Fe in the melt, consistent with experimental observations (*35*). The connection

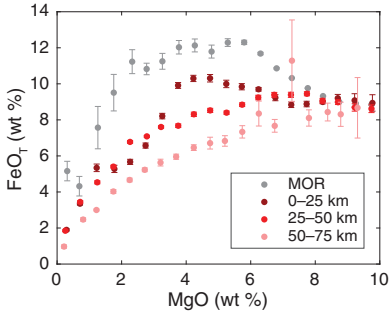

Fig. 3. FeO_T-MgO systematics in arc and mid ocean ridge (MOR) magmas. Data are presented as MgO binned (0.5 wt %) average and 2 SEM. Tholeiitic differentiation is represented by the mid-ocean ridge series (MOR). We divide arc igneous samples (mostly of Cenozoic ages) into three groups based on their modern arc crustal thickness: <25, 25 to 50, and >50 km. Arc magma compositions transition from tholeiitic to calc-alkaline as crust thickness increases. MOR data are from Keller *et al.* (*58*); arc data are from GeoRoc compilation and provided in data file S2.

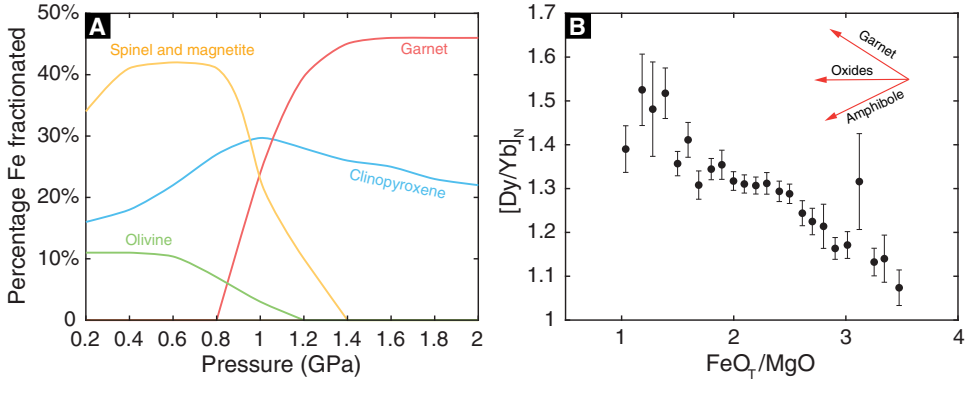

Fig. 4. Garnet control on Fe depletion. (**A**) Percentage of total initial Fe content removed by various fractionating phases after 60% crystal fractionation. Results are from pMELTS simulation of hydrous basalt crystal fractionation (fractional crystallization) under 0.2 to 2.0 GPa, 4 wt % starting water content, and a constant fO_2 of FMQ. (**B**) The extent of Fe depletion in arc magmas, as quantified by FeO_T/MgO in moderately differentiated samples of 4 ± 1 wt % MgO, correlates with garnet fractionation index $[Dy/Yb]_N$, where the subscript T denotes total Fe and N means C1 chondrite-normalized. Data are presented as FeO_T/MgO binned (0.1) average values and 2 SEM.

between calc-alkaline differentiation and garnet fractionation was first proposed by Green and Ringwood (*36*–*38*). Here, we show that the effect of garnet fractionation is borne out in global compilations of arc magma data, where Fe depletion clearly correlates with Dy/Yb (Fig. 4B), the latter being a strong tracer of garnet fractionation (*39*, *40*). Garnets in pyroxenites have been shown to have extremely low ferric Fe contents ($Fe^{3+}/\Sigma Fe < 0.01$) (*41*). Eclogite garnets have also been found to contain low ferric Fe ($Fe^{3+}/\Sigma Fe < 0.08$) (*42*, *43*). We note that although Fe^{3+} is more compatible in clinopyroxene than in garnet (*44*), clinopyroxene takes much less Fe than garnet. Collectively, fractionation of garnet-bearing cumulates at high pressure can simultaneously drive Fe depletion and increase $Fe^{3+}/\Sigma Fe$ in the derivative melt with differentiation.

To quantify the garnet fractionation effect on Fe valence in the derivative melt, we use a simplified crystal fractionation model in which the crystallizing assemblage is represented by garnet, whereas all other phases are treated as a separate nongarnet assemblage. As a minimum bound on the degree of Fe depletion, we designate the nongarnet assemblage to have bulk partition coefficients of 1 and 0.8 for Fe^{2+} and Fe^{3+}, respectively. We assume that garnet takes only Fe^{2+} and has a bulk Fe partition coefficient significantly >1. For various differentiation pressures, we explore a range of garnet mode from 0 to 30% in the fractionation assemblage, and a range from 0 to 60% Fe removal via garnet fractionation. When the garnet mode is zero, as would be the case for low-pressure differentiation, magma fO_2 remains nearly constant (Fig. 5B). When garnet mode increases and its fractionation removes over 40% of the total Fe, the magma can be progressively oxidized to at least FMQ+1, consistent with the terminal magma redox conditions constrained by observed cumulate Eu/Eu* values. Our forward-modeled Eu/Eu* trend during garnet fractionation agrees well with the observed cumulate Eu/Eu* data (Fig. 5C).

We recognize that magma oxidation and Fe depletion paths will also be influenced by Fe oxides and changing Fe partition coefficients with differentiation, which are not accounted for in our simplified model. Nevertheless, we show that garnet fractionation leads to simultaneous Fe depletion (*35*) and oxidation of the derivative melt, both of which characterize calc-alkaline differentiation. Because the mode of garnet, and thus the amount of Fe removed by garnet, increases with pressure and water content in the melt during crystal fractionation (*45*), this model explains why calc-alkaline differentiation is associated with thickened crust. Magnetite saturation should only occur after the magma is significantly oxidized by garnet fractionation, and is unlikely to be the main driver of Fe depletion in calc-alkaline series because magnetite removes ferric Fe, which reduces the fO_2 of the derivative melt and prevents the magma from remaining oxidized. Fe-oxide fractionation is a consequence of increasing fO_2. Consistent with this conclusion is that Fe oxides only appear in the differentiated cumulates, not the primitive ones. With progressive differentiation, eventual coprecipitation of magnetite and garnet may then buffer the differentiated arc magmas at a certain fO_2 above FMQ.

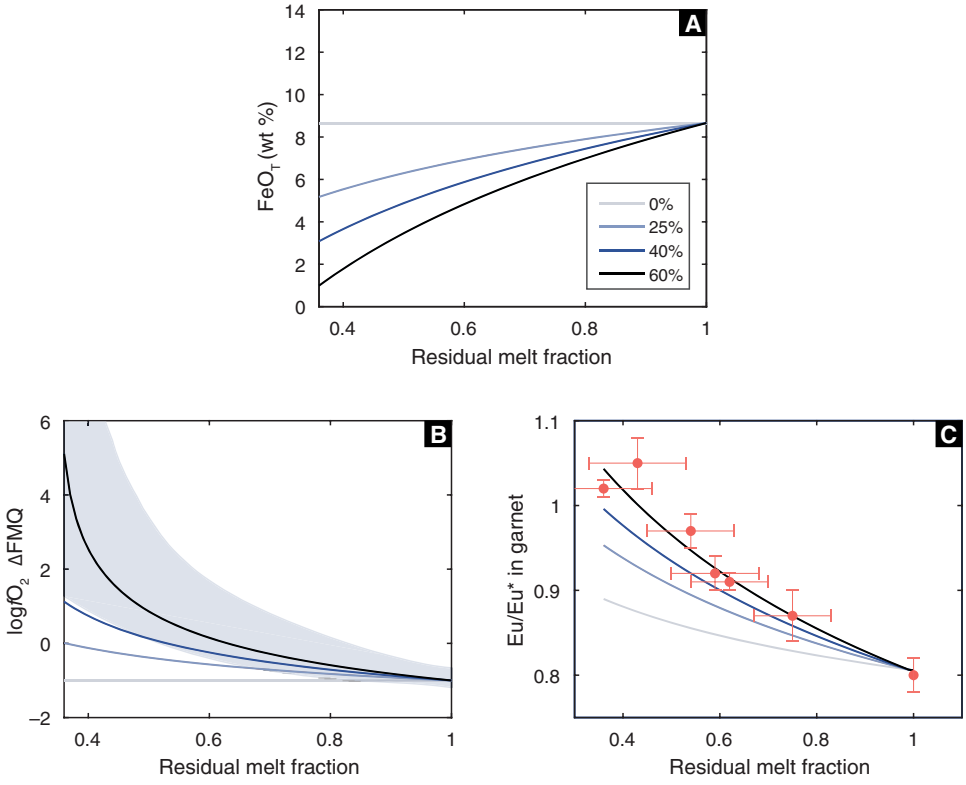

Fig. 5. Modeled garnet effect on magma redox evolution with differentiation. (**A**) Fe depletion curves assuming 0 to 60% Fe removal by garnet fractionation. (**B**) Magma fO_2 evolution curves as a function of the amount of Fe removed by garnet fractionation. Magma fO_2 paths calculated from cumulate Eu/Eu* data (shaded area) are also shown for comparison. (**C**) Calculated Eu/Eu* in cumulate garnet based on the magma fO_2 evolution curves in (B). Superimposed are the cumulate garnet Eu/Eu* data from this work.

CONCLUSIONS AND IMPLICATIONS

In summary, the Fe-depleting calc-alkaline differentiation series, which dominates the composition of the continental crust, may not be determined by initial magma redox conditions, but may instead be controlled by the effective pressure of magmatic differentiation in the crust. Our conclusions do not exclude other scenarios for generating calc-alkaline signatures, such as partial melting of eclogitic slabs, crustal contamination, and metasomatic oxidation of the sub-arc mantle (*1*, *4*, *5*), and no doubt, calc-alkaline magmas occasionally do occur in island arcs. However, the overall relationship between crustal thickness and degree of calc alkalinity appears to be a general global phenomenon and points to the dominance of upper plate thickening, or orogenic processes, in the formation of calc-alkaline magmas and Earth's continental crust (*46*–*48*). Our study provides an internally consistent mechanism for explaining this connection between oxidation and magmatic differentiation in thick crust.

Important implications follow. Iron depletion driven by garnet fractionation under reduced conditions will lead to sulfide saturation in the magma because sulfide solubility decreases with FeO content in the melt, thereby driving extensive sulfide coprecipitation with the cumulates (*47*, *49*, *50*). Deep continental arc cumulates may be an important reservoir for chalcophile elements and unradiogenic Pb isotopes (*47*, *51*, *52*). If these cumulates were to founder back into the mantle, owing to their high densities (*14*, *52*–*55*), then the progressive growth of the continental crust would lead to a flux of reduced materials to the mantle, leaving behind a more oxidized continental crust. We thus envision that the formation of continental crust results in a gravity-driven redox filter, which may have influenced Earth's surface redox evolution by limiting the magmatic output of ferrous Fe and sulfides (*56*, *57*).

MATERIALS AND METHODS

Details about the samples, analytical techniques, and modeling are provided in the Supplementary Materials. Data are provided in data files S1 to S3.

SUPPLEMENTARY MATERIALS

Supplementary material for this article is available at http://advances.sciencemag.org/cgi/content/full/4/5/eaar4444/DC1

Supplementary Materials and Methods

Supplementary Text

fig. S1. Comparison between our measured Eu/Eu* in glass standards BCR-2G, BIR-1G, KL2-G, ML3B-G, and StHs6/80-G.

fig. S2. Long-term (8 months) reproducibility in the analysis of glass standards BIR-1G and BCR-2G.

fig. S3. Chondrite-normalized REE/FeO values for clinopyroxene.

fig. S4. Chondrite-normalized REE/FeO values for garnet.

fig. S5. Mean Eu/Eu* versus MgO in global arc lavas.

fig. S6. Calculated logfO_2 as a function of optical basicity assuming Eu/Eu* = 0.8 in garnet.

fig. S7. Mineral Mg# versus whole-rock Mg# in the cumulates documented in this work.

fig. S8. Melt-cumulate Mg# correlation simulated by pMELTS at 2 GPa, 4 wt % H_2O, and various oxygen fugacities.

fig. S9. Observed K_2O-Mg# correlation in arc magmas, parameterized by an exponential function shown in the figure.

fig. S10. Error propagation by Monte Carlo resampling.

fig. S11. Sensitivity test of calculated D_{Eu}/D_{Eu^*} and redox paths to the value of D_{Eu^*} used in the crystal fractionation model.

fig. S12. Calculated optical basicity (Λ) as a function of Mg# in arc magmas.

data file S1. In-situ mineral composition data and cumulate whole-rock data.

data file S2. Primitive arc magma compositions.

data file S3. Global arc igneous rock compilation.

References (*59*–*63*)

REFERENCES AND NOTES

1. I. S. E. Carmichael, The redox states of basic and silicic magmas: A reflection of their source regions? *Contrib. Mineral. Petrol.* **106**, 129–141 (1991).
2. M. M. Zimmer, T. Plank, E. H. Hauri, G. M. Yogodzinski, P. Stelling, J. Larsen, B. Singer, B. Jicha, C. Mandeville, C. J. Nye, The role of water in generating the calc-alkaline trend: New volatile data for aleutian magmas and a new tholeiitic index. *J. Petrol.* **51**, 2411–2444 (2010).
3. R. L. Rudnick, S. Gao, Composition of the continental crust, in *Treatise on Geochemistry*, H. D. Holland, K. K. Turekian, Eds. (Elsevier, ed. 2, 2014), pp. 1–51.
4. J. C. M. de Hoog, K. H. Hattori, R. P. Hoblitt, Oxidized sulfur-rich mafic magma at Mount Pinatubo, Philippines. *Contrib. Mineral. Petrol.* **146**, 750–761 (2004).
5. K. A. Kelley, E. Cottrell, Water and the oxidation state of subduction zone magmas. *Science* **325**, 605–607 (2009).
6. N. Dauphas, P. R. Craddock, P. D. Asimow, V. C. Bennett, A. P. Nutman, D. Ohnenstetter, Iron isotopes may reveal the redox conditions of mantle melting from Archean to Present. *Earth Planet. Sci. Lett.* **288**, 255–267 (2009).
7. C.-T. A. Lee, P. Luffi, V. Le Roux, R. Dasgupta, F. Albaréde, W. P. Leeman, The redox state of arc mantle using Zn/Fe systematics. *Nature* **468**, 681–685 (2010).
8. G. Mallmann, H. S. C. O'Neill, The crystal/melt partitioning of V during mantle melting as a function of oxygen fugacity compared with some other elements (Al, P, Ca, Sc, Ti, Cr, Fe, Ga, Y, Zr and Nb). *J. Petrol.* **50**, 1765–1794 (2009).
9. C.-T. A. Lee, W. P. Leeman, D. Canil, Z.-X. A. Li, Similar V/Sc systematics in MORB and arc basalts: Implications for the oxygen fugacities of their mantle source regions. *J. Petrol.* **46**, 2313–2336 (2005).
10. A. D. Burnham, A. J. Berry, H. R. Halse, P. F. Schofield, G. Cibin, J. F. W. Mosselmans, The oxidation state of europium in silicate melts as a function of oxygen fugacity, composition and temperature. *Chem. Geol.* **411**, 248–259 (2015).
11. M. E. Erdman, C.-T. A. Lee, A. Levander, H. Jiang, Role of arc magmatism and lower crustal foundering in controlling elevation history of the Nevadaplano and Colorado Plateau: A case study of pyroxenitic lower crust from central Arizona, USA. *Earth Planet. Sci. Lett.* **439**, 48–57 (2016).
12. D. Smith, R. J. Arculus, J. E. Manchester, G. N. Tyner, Garnet-pyroxene-amphibole xenoliths from Chino Valley, Arizona, and implications for continental lithosphere below the Moho. *J. Geophys. Res. Solid Earth* **99**, 683–696 (1994).
13. C.-T. A. Lee, X. Cheng, U. Horodyskyj, The development and refinement of continental arcs by primary basaltic magmatism, garnet pyroxenite accumulation, basaltic recharge and delamination: Insights from the Sierra Nevada, California. *Contrib. Mineral. Petrol.* **151**, 222–242 (2006).
14. M. N. Ducea, J. B. Saleeby, The age and origin of a thick mafic–ultramafic keel from beneath the Sierra Nevada batholith. *Contrib. Mineral. Petrol.* **133**, 169–185 (1998).
15. M. Tang, W. F. McDonough, R. D. Ash, Europium and strontium anomalies in the MORB source mantle. *Geochim. Cosmochim. Acta* **197**, 132–141 (2017).
16. J. H. Bédard, Parameterizations of calcic clinopyroxene—Melt trace element partition coefficients. *Geochem. Geophys. Geosyst.* **15**, 303–336 (2014).
17. J. S. Herrin, C.-T. A. Lee, D. W. Mittlefehldt, Genesis of augite-bearing ureilites: Evidence from LA-ICP-MS analyses of pyroxenes and olivine, *39th Lunar and Planetary Science Conference*, League City, Texas, 10 to 14 March 2008.
18. A. Bézos, E. Humler, The $Fe^{3+}/\Sigma Fe$ ratios of MORB glasses and their implications for mantle melting. *Geochim. Cosmochim. Acta* **69**, 711–725 (2005).
19. V. C. Kress, I. S. E. Carmichael, The compressibility of silicate liquids containing Fe_2O_3 and the effect of composition, temperature, oxygen fugacity and pressure on their redox states. *Contrib. Mineral. Petrol.* **108**, 82–92 (1991).
20. A. J. Berry, G. A. Stewart, H. S. C. O'Neill, G. Mallmann, J. F. W. Mosselmans, A re-assessment of the oxidation state of iron in MORB glasses. *Earth Planet. Sci. Lett.* **483**, 114–123 (2018).
21. H. Fujimaki, M. Tatsumoto, K.-i. Aoki, Partition coefficient of Hf, Zr, and REE between phenocrysts and groundmasses, in *Proceedings of the 14th Lunar and Planetary Science Conference*, Houston, Texas, 15 February 1984.
22. K. T. M. Johnson, Experimental cpx/and garnet/melt partitioning of REE and other trace elements at high pressures: Petrogenetic implications. *Mineral. Mag. A* **58**, 454–455 (1994).
23. J. Berndt, J. Koepke, F. Holtz, An experimental investigation of the influence of water and oxygen fugacity on differentiation of MORB at 200 MPa. *J. Petrol.* **46**, 135–167 (2004).
24. C.-T. A. Lee, T. C. Lee, C.-T. Wu, Modeling the compositional evolution of recharging, evacuating, and fractionating (REFC) magma chambers: Implications for differentiation of arc magmas. *Geochim. Cosmochim. Acta* **143**, 8–22 (2014).
25. H. Kuno, Lateral variation of basalt magma type across continental margins and Island Arcs. *Bull. Volcanol.* **29**, 195–222 (1966).
26. H. Kuno, Origin of andesite and its bearing on the Island arc structure. *Bull. Volcanol.* **32**, 141–176 (1968).

27. M. J. Farner, C.-T. A. Lee, Effects of crustal thickness on magmatic differentiation in subduction zone volcanism: A global study. *Earth Planet. Sci. Lett.* **470**, 96–107 (2017).
28. M. Chiaradia, Copper enrichment in arc magmas controlled by overriding plate thickness. *Nat. Geosci.* **7**, 43–46 (2014).
29. S. G. Rotolo, F. Castorina, Transition from mildly-tholeiitic to calc-alkaline suite: The case of Chichontepec volcanic centre, El Salvador, Central America. *J. Volcanol. Geotherm. Res.* **86**, 117–136 (1998).
30. K.-i. Aoki, Y. Oji, Calc-alkaline volcanic rock series derived from alkali-olivine basalt magma. *J. Geophys. Res.* **71**, 6127–6135 (1966).
31. M. Chiaradia, Crustal thickness control on Sr/Y signatures of recent arc magmas: An Earth scale perspective. *Sci. Rep.* **5**, 8115 (2015).
32. L. Profeta, M. N. Ducea, J. B. Chapman, S. R. Paterson, S. M. H. Gonzales, M. Kirsch, L. Petrescu, P. G. DeCelles, Quantifying crustal thickness over time in magmatic arcs. *Sci. Rep.* **5**, 17786 (2015).
33. E. J. Chin, K. Shimizu, G. M. Bybee, M. E. Erdman, On the development of the calc-alkaline and tholeiitic magma series: A deep crustal cumulate perspective. *Earth Planet. Sci. Lett.* **482**, 277–287 (2018).
34. M. S. Ghiorso, M. M. Hirschmann, P. W. Reiners, V. C. Kress III, The pMELTS: A revision of MELTS for improved calculation of phase relations and major element partitioning related to partial melting of the mantle to 3 GPa. *Geochem. Geophys. Geosyst.* **3**, 1–35 (2002).
35. R. Alonso-Perez, O. Müntener, P. Ulmer, Igneous garnet and amphibole fractionation in the roots of island arcs: Experimental constraints on andesitic liquids. *Contrib. Mineral. Petrol.* **157**, 541–558 (2009).
36. T. H. Green, Crystallization of calc-alkaline andesite under controlled high-pressure hydrous conditions. *Contrib. Mineral. Petrol.* **34**, 150–166 (1972).
37. T. H. Green, A. E. Ringwood, Genesis of the calc-alkaline igneous rock suite. *Contrib. Mineral. Petrol.* **18**, 105–162 (1968).
38. T. H. Green, A. E. Ringwood, Origin of garnet phenocrysts in calc-alkaline rocks. *Contrib. Mineral. Petrol.* **18**, 163–174 (1968).
39. R. L. Rudnick, S. R. Taylor, Geochemical constraints on the origin of Archaean tonalitic-trondhjemitic rocks and implications for lower crustal composition. *Geol. Soc. Lond. Spec. Publ.* **24**, 179–191 (1986).
40. J. Davidson, S. Turner, H. Handley, C. Macpherson, A. Dosseto, Amphibole "sponge" in arc crust? *Geology* **35**, 787–790 (2007).
41. D. Canil, H. S. C. O'Neill, Distribution of ferric iron in some upper-mantle assemblages. *J. Petrol.* **37**, 609–635 (1996).
42. S. Aulbach, A. B. Woodland, P. Vasilyev, M. E. Galvez, K. S. Viljoen, Effects of low-pressure igneous processes and subduction on $Fe^{3+}/\Sigma Fe$ and redox state of mantle eclogites from Lace (Kaapvaal craton). *Earth Planet. Sci. Lett.* **474**, 283–295 (2017).
43. Y.-L. Li, Y.-F. Zheng, B. Fu, Mössbauer spectroscopy of omphacite and garnet pairs from eclogites: Application to geothermobarometry. *Am. Mineral.* **90**, 90–100 (2005).
44. V. Stagno, D. J. Frost, C. McCammon, H. Mohseni, Y. Fei, The oxygen fugacity at which graphite or diamond forms from carbonate-bearing melts in eclogitic rocks. *Contrib. Mineral. Petrol.* **169**, 16 (2015).
45. J.-F. Moyen, G. Stevens, Experimental constraints on TTG petrogenesis: Implications for Archean geodynamics, in *Archean Geodynamics and Environments*, K. Benn, J.-C. Mareschal, K. C. Condie, Eds. (American Geophysical Union, 2013), pp. 149–175.
46. L. Karlstrom, J. Dufek, M. Manga, Magma chamber stability in arc and continental crust. *J. Volcanol. Geotherm. Res.* **190**, 249–270 (2010).
47. C.-T. A. Lee, P. Luffi, E. J. Chin, R. Bouchet, R. Dasgupta, D. M. Morton, V. Le Roux, Q.-z. Yin, D. Jin, Copper systematics in arc magmas and implications for crust-mantle differentiation. *Science* **336**, 64–68 (2012).
48. C.-T. A. Lee, D. M. Morton, R. W. Kistler, A. K. Baird, Petrology and tectonics of Phanerozoic continent formation: From island arcs to accretion and continental arc magmatism. *Earth Planet. Sci. Lett.* **263**, 370–387 (2007).
49. D. R. Baker, R. Moretti, Modeling the solubility of sulfur in magmas: A 50-year old geochemical challenge. *Rev. Mineral. Geochem.* **73**, 167–213 (2011).
50. S. Ding, R. Dasgupta, K. Tsuno, Sulfur concentration of martian basalts at sulfide saturation at high pressures and temperatures – Implications for deep sulfur cycle on Mars. *Geochim. Cosmochim. Acta* **131**, 227–246 (2014).
51. S. Huang, C.-T. A. Lee, Q.-Z. Yin, Missing lead and high $^3He/^4He$ in ancient sulfides associated with continental crust formation. *Sci. Rep.* **4**, 5314 (2014).
52. O. Jagoutz, M. W. Schmidt, The composition of the foundered complement to the continental crust and a re-evaluation of fluxes in arcs. *Earth Planet. Sci. Lett.* **371–372**, 177–190 (2013).
53. C.-T. A. Lee, Physics and chemistry of deep continental crust recycling, in *Treatise on Geochemistry,* H. D. Holland, K. K. Turekian, Eds. (Elsevier, ed. 2, 2014), pp. 423–456.
54. O. Jagoutz, M. D. Behn, Foundering of lower island-arc crust as an explanation for the origin of the continental Moho. *Nature* **504**, 131–134 (2013).
55. R. W. Kay, S. M. Kay, Delamination and delamination magmatism. *Tectonophysics* **219**, 177–189 (1993).
56. C.-T. A. Lee, L. Y. Yeung, N. R. McKenzie, Y. Yokoyama, K. Ozaki, A. Lenardic, Two-step rise of atmospheric oxygen linked to the growth of continents. *Nat. Geosci.* **9**, 417–424 (2016).
57. M. A. Smit, K. Mezger, Earth's early O_2 cycle suppressed by primitive continents. *Nat. Geosci.* **10**, 788–792 (2017).
58. C. B. Keller, B. Schoene, M. Barboni, K. M. Samperton, J. M. Husson, Volcanic-plutonic parity and the differentiation of the continental crust. *Nature* **523**, 301–307 (2015).
59. M. H. Krieger, S. C. Creasey, R. F. Marvin, Ages of some Tertiary andesitic and latitic volcanic rocks in the Prescott-Jerome area, north-central Arizona. *US Geol. Survey Prof. Pap.* **750**, 157–160 (1971).
60. R. D. Shannon, Revised effective ionic radii and systematic studies of interatomic distances in halides and chalcogenides. *Acta Crystallogr. A* **32**, 751–767 (1976).
61. S.-s. Sun, W. F. McDonough, Chemical and isotopic systematics of oceanic basalts: Implications for mantle composition and processes. *Geol. Soc. Lond. Spec. Publ.* **42**, 313–345 (1989).
62. J. A. Duffy, A review of optical basicity and its applications to oxidic systems. *Geochim. Cosmochim. Acta* **57**, 3961–3970 (1993).
63. GeoRoc online database, http://georoc.mpch-mainz.gwdg.de/georoc/.

Acknowledgments: We thank J. Gao for helping us with coding in the pMELTS simulations. We also thank X. Chu, A. Burnham, and G. Costin for the discussions. We thank G. Gaetani for handling the manuscript, and D. Canil and two other anonymous reviewers for their constructive comments. **Funding:** This project was supported by Frontiers of Earth Systems and Dynamics (NSF OCE-1338842). **Author contributions:** G.E. made the first discovery of the Eu/Eu*-Mg# correlation in preliminary whole-rock data. M.E. did petrographic and whole-rock characterization to study the petrogenesis of the cumulates. M.T. designed the in situ analytical method, collected the data, and built the models. C.-T.A.L. and M.T interpreted the data and wrote the manuscript. **Competing interests:** The authors declare that they have no competing interests. **Data and materials availability:** All data needed to evaluate the conclusions in the paper are present in the paper and/or the Supplementary Materials. Additional data related to this paper may be requested from the authors.

Submitted 8 November 2017
Accepted 3 April 2018
Published 16 May 2018
10.1126/sciadv.aar4444

Citation: M. Tang, M. Erdman, G. Eldridge, C.-T. A. Lee, The redox "filter" beneath magmatic orogens and the formation of continental crust. *Sci. Adv.* **4**, eaar4444 (2018).

The redox "filter" beneath magmatic orogens and the formation of continental crust

Ming Tang, Monica Erdman, Graham Eldridge and Cin-Ty A. Lee

Sci Adv **4** (5), eaar4444.
DOI: 10.1126/sciadv.aar4444